
Article:
Liu, J, Yin, L, Chandler, JH orcid.org/0000-0001-9232-4966 et al. (3 more authors) (2021) A Dual-bending Endoscope with Shape-lockable Hydraulic Actuation and Water-jet Propulsion for Gastrointestinal Tract Screening. The International Journal of Medical Robotics and Computer Assisted Surgery, 17 (1). pp. 1-13. ISSN 1478-5951

https://doi.org/10.1002/rcs.2197

Jianbin Liu (Orcid ID: 0000-0001-9712-2722)
Linkun Yin (Orcid ID: 0000-0002-8956-6603)
James Chandler (Orcid ID: 0000-0001-9232-4966)
Pietro Valdastri (Orcid ID: 0000-0002-2280-5438)
Siyang Zuo (Orcid ID: 0000-0003-4257-7978)

A Dual-bending Endoscope with Shape-lockable Hydraulic Actuation and Water-jet Propulsion for Gastrointestinal Tract Screening

Jianbin Liu[1], Linkun Yin[1], James H. Chandler[2], Xin Chen[3], Pietro Valdastri[2], Siyang Zuo[1†]

[1]Key Laboratory of Mechanism Theory and Equipment Design, Ministry of Education, Tianjin University, Tianjin, China

[2]Institute of Robotics, Autonomous Systems and Sensing, School of Electronic and Electrical Engineering, University of Leeds, Leeds, U.K.

[3]Tianjin Medical University General Hospital

Abstract

A dual-bending hydraulic endoscope with shape-locking function to perform inexpensive gastric screening is developed in this study. The endoscope employs a custom microvalve to switch between hydraulic actuation of a spatial bending fluidic actuator and water-jet actuation. Three alloy wires with buckle attachments are connected to a pneumatic balloon which facilitates reversible shape-locking of the actuator, and thus supports stable scanning by water-jet actuation. Experiments demonstrated a 58% increase in the workspace after introduction of the water-jet. Stiffness tests of the shape-locking mechanism revealed that the device in rigid state achieved more than three times the load-locking ability of flexible state. Length of insertion tube is 600 mm, with a maximum outer diameter of 13 mm. Distal tip of the tube has an internal charge-coupled device camera for inspection. The prototype was validated through phantom experiments, demonstrating the potential clinical value of the endoscope system.

† **Corresponding author:** Siyang Zuo, e-mail: siyang_zuo@tju.edu.cn

This article has been accepted for publication and undergone full peer review but has not been through the copyediting, typesetting, pagination and proofreading process, which may lead to differences between this version and the Version of Record. Please cite this article as doi: 10.1002/rcs.2197.

Keywords: *Robotic endoscopy, shape-locking mechanism, microvalve, gastric cancer screening, water-jet.*

INTRODUCTION

Cancer is one of the leading causes of death worldwide, with gastric cancer representing the fifth most common type of cancer with 1 million new cases in 2018. It is also the third most common cause of cancer-related death, with 793,000 deaths [1]. Furthermore, gastric cancer exhibits significant socioeconomic and geographic dependence, with more than 70% cases concentrated in low- and middle-income countries [2-3]. Studies have shown that early detection of precancerous lesions, often via endoscopic screening, is important for reducing the mortality rate of gastric cancer [4-5]. However, commercial flexible endoscopes are sophisticated medical devices that require frequent and expensive maintenance. Therefore, their implementation within low-income and rural regions is challenging due to their high cost, complex sterilization process [6, 7], and poor portability. Consequently, regions with lower socioeconomic status often lack the resources to procure and properly maintain endoscopes [8]. Thus, it is necessary to develop endoscopic platforms that are low-cost, disposable, and portable, with the primary goal of reducing gastric cancer-related mortality among low- and middle-income communities through wider access to regular screening programs.

A number of approaches to low-cost endoscope design have been proposed; including cable driven [9], tethered capsules [10-11], and pneumatically driven [12-13] devices. In addition to these, water-jet driven endoscopes represent a prevalent approach, with the advantage of low-cost and disposable features and water-jet based orientation control [14-17]. The disposable, water-jet-actuated design makes the approach viable for application in gastric screening at low- and middle-income countries. However, the capsule has a few limitations arising from an unstable platform and a single-bending section. Due to the excessive flexibility of the tethered structure and unstable motion of the water-jet, attempting to observe a target stably or even manipulate tissues during endoscopic procedures is difficult without integration of sensing and closed-loop control [17]. To improve actuation stability, a water-jet outer sheath with a variable stiffness mechanism and braided structure was developed [18]. However, the bending section cannot flex reach large angles, making it challenging to examine the cardia and lesser curvature of the stomach. Furthermore, due to the phase-

change material mechanism employed, rapid stiffness variation and shape locking is precluded; which could result in extended procedural times and the associated injection of an excess of water into the body.

To overcome some of the existing disadvantages of water-jet endoscope mechanisms, other driving methods may be considered to work together with water-jet. Wire or tendon drive is widely used in medical robotics as it can realize high accuracy and compact designs. However, it is not well suited for low-cost endoscope applications as the insertion part cannot easily be made disposable. The procedures for connecting, assembling and tightening of driving wires are complex and time-consuming, and tendon-sheath mechanisms represent a higher cost than the proposed method.

The driving methods used in continuum and soft robotics draw much attention of researchers in medical robot design [19-20] due to them being capable of safe, dynamic, and flexible bending performance; owing to their natural compliance [21]. In addition, unlike piston-based or cable-driven systems, soft robots have low friction between their movable parts [22-23]. Hence, they can achieve smooth motion and precise positioning. Among the many soft robot actuation methods, hydraulic actuation offers several advantages for the proposed application. The actuator can be miniaturized depending on the application constraints; the liquid flow acts as a natural damper, preventing rapid pressure variations that may damage the robot or the surrounding tissue [24]; and hydraulic microvalves may be employed to produce single-input, multi-output systems [25].

Stiffness variation and shape-locking is another important requirement for many medical soft robots; as a stable platform is often needed for more accurate local screening or surgical procedures. Wire tension and pneumatic mechanisms are the two major methods for shape-locking or variable stiffness medical soft robots [26-31]. A highly articulated robotic probe (HARP) with shape-lockable function was presented and applied in endoluminal surgery [26]. By pulling back the three wires 120 degrees apart along the device, its shape can be locked due to the increasing friction between the tube connecting parts. The wire tension method has the advantage of easy actuation, but often suffers with wire extension and breakage. Pneumatic methods represent a simpler way to induce stiffness variation and shape locking. A “snake belly” structure [27] and a “dragon skin” mechanism [28] were developed by Zuo et al. to lock shape of medical instruments by engaging specifically designed tooth links or bellows tubes under application of negative pressure. Other pneumatic mechanisms include layer

jamming [30], granular jamming structures [31] and fiber jamming structures [32]. The disadvantages of pneumatic approaches are the large sizes required for inner body operations and the small locking power produced.

As a logical iteration of these types of soft robots, we propose a novel dual-bending hydraulic endoscope with a spatial bending fluidic actuator (SBFA) and water-jet that can achieve effective and safe actuation of the robot for endoscopic procedures (Fig. 1). A specially designed microvalve, whose on/off state is controlled by input pressure, is utilized to alter between single-bending and water-jet-enhanced dual-bending motions. A pneumatic shape-locking mechanism based on alloy wires with buckle attachments has been developed and integrated to increase the stiffness of the platform instantly and reversibly, and thus help the distal tip achieve a more stable scanning motion. The specific features of the new system are:

1. Integration of hydraulic and water-jet mechanisms to achieve dual-bending while ensuring safety. Combination of the two mechanisms increases the workspace for the endoscope. In addition, introducing of the bending mechanism significantly reduces the volume of water ejected into the patient's stomach compared with traditional water-jet design, which is because much portion of the inspection work can be performed by the hydraulic bending mechanism alone.

2. A new, custom pressure controlled microvalve transforms hydraulic actuation to water-jet actuation. A certain range of bending can be achieved through hydraulic actuation of the SBFA alone (i.e. with the microvalve closed). When a larger bending curvature is required, the microvalve can be opened to enable the water-jet mechanism to further increase the bending range of the endoscope. As the microvalves are controlled using the input water pressure lines, simple system operation is maintained.

3. The position of the soft SBFA can be reversibly fixed via the shape-locking mechanism. A pneumatically driven balloon radially expands to engage the buckle attachments of three alloy wires with its outer wall; providing a stable platform for water-jet tip actuation to scan the targeted area. The shape locking system is integrated into the endoscope without increasing the outer diameter or invade the inner channel for camera wires.

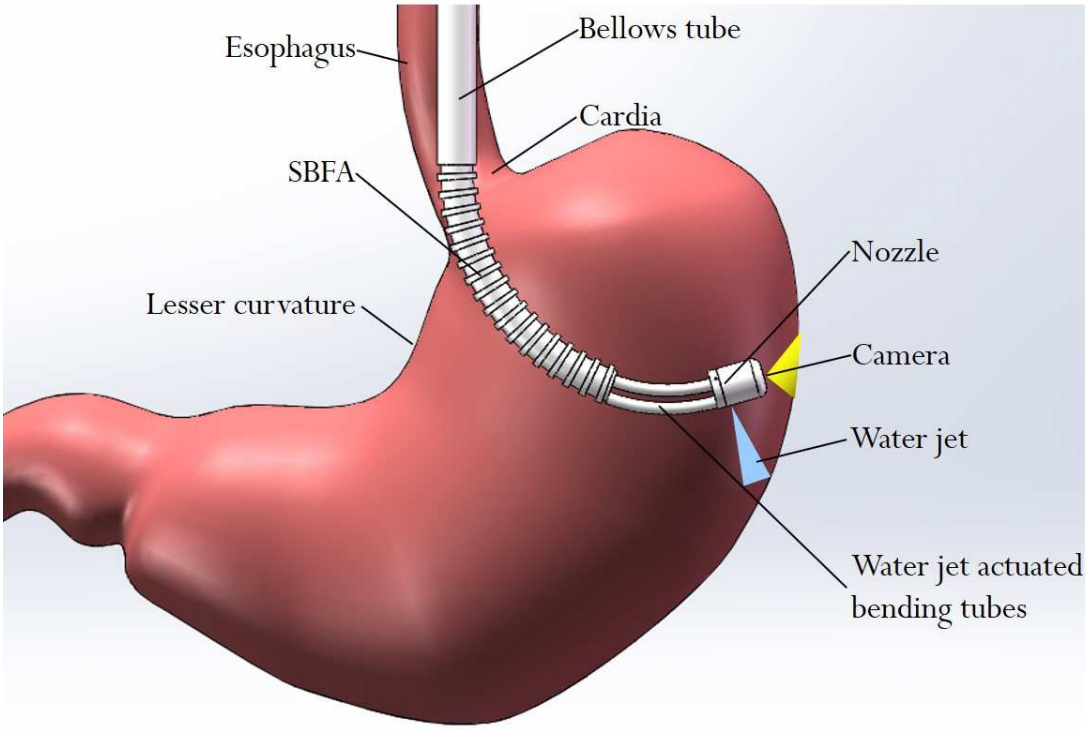

Fig. 1. Endoscope for gastric screening.

Prototype Design and Fabrication

The design considerations of the endoscope are shown in Tab. I. The shaft of the endoscope is mainly composed of three parts (Fig. 2(a))—a bellows tube, an SBFA with shape-locking function, and water-jet steerable tip. The prototype has a maximum outer diameter of 13 mm and a length of 600 mm. Pressurized water causes the SBFA to expand and bend. As the pressure of the water increases above a threshold, the microvalve opens and the nozzle is actuated by the water-jet, which increases the bending range and helps scan the targeted area. The designed endoscope with water-jet-enhanced bending mechanism is shown in Fig. 2(b). The tip of the endoscope can turn by an angle of up to 180°, with the proposed dual-bending design.

TABLE I. Design requirements of endoscope platform with water-jet mechanism.

Diameter of esophagus	Bending length	Horizontal workspace projection radius	Exhaust pressure	Stability
2–3 cm [32]	≥ 150 mm [33]	≥ 100 mm [33]	≤ 3 bar [34]	Variable stiffness

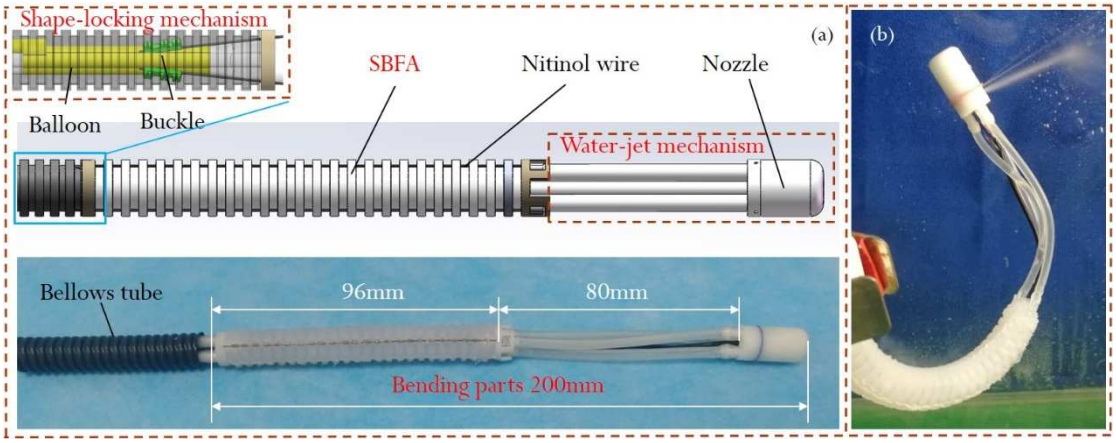

Fig. 2. (a) Structural design of the endoscope. (b) The designed endoscope with water-jet-enhanced bending mechanism.

The structural parameters of this work and five commercial devices are listed as Tab. II. A smaller outer diameter (under 10mm) and longer insertion part (over 1m) of the developed endoscope are preferred to further minimize the invasive of the procedure and approach more deep area in gastrointestinal track. Nevertheless, the current outer diameter and length of the prototype should be acceptable for clinical usage, since it is superior to some of the current devices. The 60cm working length was determined according to the requirements of phantom test in this work. One benefit of the presented hydraulic-drive design, is the relative simplicity in fabricating the insertion part to arbitrary length (e.g. longer). This is specifically enabled because there are only the water tubes and the camera wires inside the bellows tube, and no reliance on cable layout and tensioning.

Main advantage of this work is in price, which is perfect for low-income regions. The hardware price of the whole developed equipment is $800, and the price of the insertion part is $40. However, total price of GIF-Q260 (Olympus, Japan) system is higher than $440, 000. The advantage of this work in commercial cost is significant.

TABLE II. Structural parameters comparison between commercial endoscopes and this work.

	Manufacturer	Outer Diameter (mm)	Length(cm)
GIF-Q260	Olympus	9.2	103
GIF-2TQ260M	Olympus	11.7	103
ViaCath	Hansen Medical	18	100
DDES	Boston Scientific	16	55
Incisionless Operating Platform	USGI	18	110
This work	-	13	60

Spatial Bending Fluidic Actuator (SBFA)

The SBFA has an outer diameter of 13 mm and a central channel for the passage of tools. The three parallel chambers of the SBFA can be pressurized individually and are uniformly distributed around the central axis. Fig. 3(a) illustrates the structure of the SBFA and the cross-section of an individual chamber. The anisotropic elongation among the three chambers causes the SBFA to bend, as illustrated in Fig. 3(b). There is an inextensible line (wire of the camera) along the center of the SBFA that constrains its elongation.

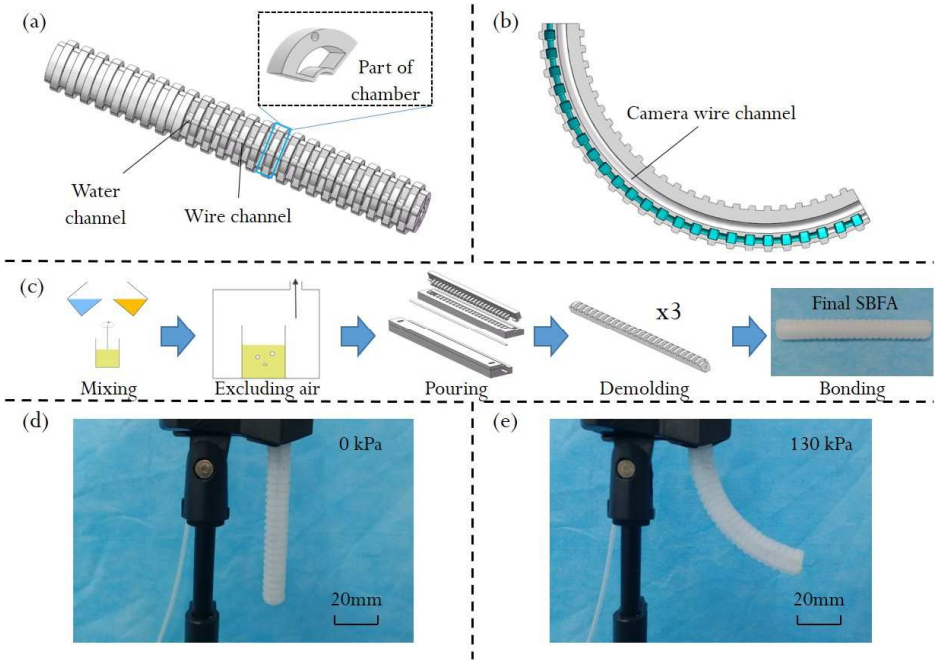

Fig. 3. (a) SBFA structural design. (b) Sectional view of the camera-wire channel in the bending state. (c) Fabrication process of the SBFA. (d) Fabricated SBFA in the unactuated state. (e) Bending state of the SBFA with one actuated channel.

The fabrication process of the SBFA is illustrated in Fig. 3(c). Three identical chambers were manufactured by casting silicone rubber (Dragon Skin 20, Smooth-On Inc., USA) in a two-part 3D-printed mold. Due to the complexity of design, each chamber was molded separately in molds designed to reduce the number of fabrication steps and maintain the integrity of the chamber. To mold each chamber, the two-part silicone was first mixed in equal proportion by weight and degassed in a vacuum chamber to remove air bubbles. Prior to casting, white petroleum jelly was applied to the surface of the molds to act as a releasing agent. The silicone prepolymer was subsequently poured carefully into the mold and degassed a second time in a vacuum chamber to remove any residual air bubbles trapped during the pouring process. The

molds were subsequently closed and cured at room temperature for 6 h before demolding.

Three identical chambers were fabricated following the above steps, and then bonded together in axisymmetric alignment using additional silicone rubber (Dragon Skin 20, Smooth-On Inc., USA.) as bonding agent. Each chamber is molded using a two-part mold with central insert to create the internal cavity. Medical tubes (outer diameter = 4 mm; inner diameter = 2 mm) were attached to each of the three chambers to allow independent supply of pressurized water. The assembled SBFA, shown in Fig. 3(d), has a length of 96 mm, a maximum diameter of 13 mm, and a total mass of 4.2 g. Actuation of the SBFA under pressurization of a single chamber to 130 kPa is shown in Fig. 3(e).

Water-jet Mechanism

The block diagram of the water-jet mechanism is shown in Fig. 4(a). Compressed air is used to pressurize water in a water tank (Fig. 4(b)). A pressure-regulating valve is installed at the air inlet of the water tank to adjust the air pressure. Water is delivered from the tank to a distribution joint. By turning on and off the two-position, three-way solenoid valves connected to the three channels, pressurized water was pumped into the tubes, which helps achieve different bending motions. When the solenoid valve is closed, the corresponding passage of the body part under observation is connected to zero pressure. When the solenoid valve is opened, the corresponding passage is connected to the pressurized water path, which actuates the scanning motion. The actuation response time mainly depends on the speed of the directional valve, which is within 100ms. An automatic interface (LabVIEW, National Instruments) was developed to control the water-jet system from a standard computer.

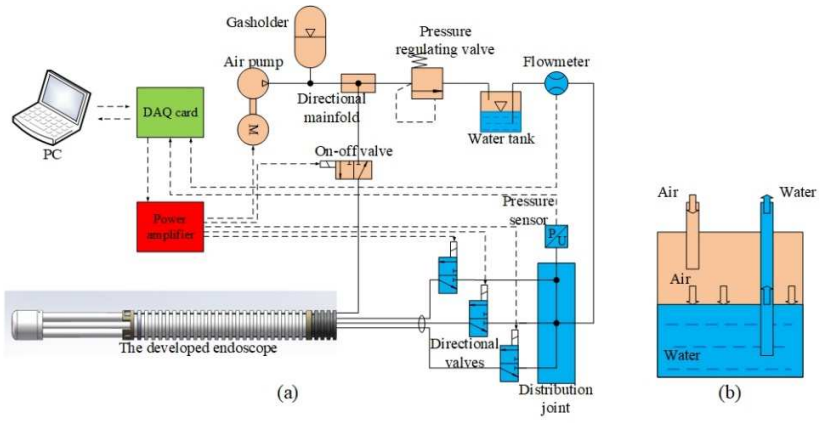

Fig. 4. (a) Block diagram of the water-jet system. (b) Structure of the water tank.

As shown in Fig. 5(a), three microvalves in the nozzle corresponding to three channels are the key components for switching between single-bending and water-jet-enhanced dual-bending motions. The microvalve, which utilizes the elastic properties of a soft membrane, is specially designed and fabricated to meet the requirements of this application. When the microvalve is closed, as shown in Fig. 5(b), the elastic rubber membrane is pretensioned to block the flow of water. The valve remains closed under pressures lower than the actuating pressure range (> 130 kPa). As the water pressure rises, the membrane is pushed open. Then, pressurized water is ejected from the nozzle, actuating the bending of the endoscope. The opening state of the microvalve is shown in Fig. 5(c). With the valve closed, no leakage occurs as the soft membrane material completely blocks the flow. The endoscope can achieve three directional bending motions with the nozzle design. The diameter and length of the nozzle are 13 mm and 20 mm, respectively.

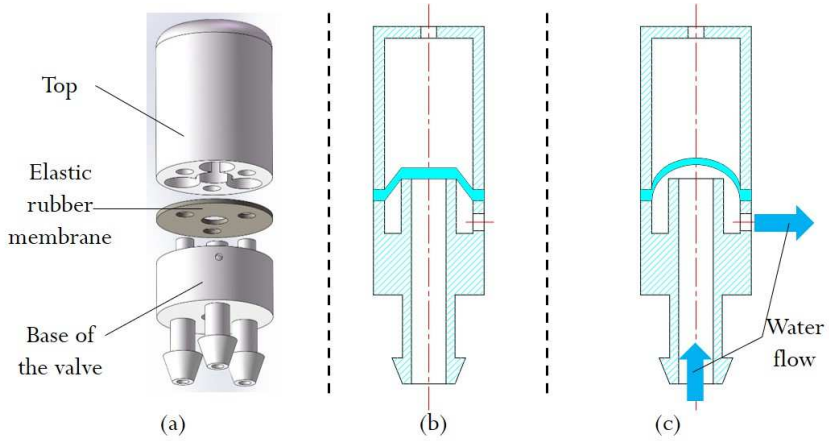

Fig. 5. (a) Nozzle structure design. (b) Closing state of the microvalve. (c) Opening state of the microvalve.

Shape-locking Mechanism

The shape-locking mechanism is shown in Fig. 6(a). Three nickel–titanium alloy wires guided by small copper eyelets are routed along the length of the SBFA parallel to the central axis. The copper eyelets reduce the friction between the alloy wire and the SBFA, and thus promote smooth bending. The proximal end of each alloy wire is terminated with a buckle structure (Fig. 6(b)), while the distal end is terminated and constrained using an aluminum sleeve. As shown in Fig. 6(b-c), a balloon (inflated with pressurized air) is used to push the small sliding buckles of the alloy wires radially to engage them with the inner wall of the bellows structure; reversibly locking the shape

of the SBFA and providing a stable platform for the water-jet tip. Furthermore, after the SBFA is locked, the tip position can be adjusted by water-jet in a continuous fashion, therefore, discreteness of the shape-locking mechanism does not limit the possible space that the device can reach. A conversion joint is used to connect the bellows with the SBFA and to act as a manifold for routing the water channels inside the bellows to the inlet of the SBFA. Specifically, the conversion joint gives a 60° rotation (around the central axis) for each water channel, as marked in Fig 6(a), to give enough clearance for the shape locking mechanism in the bellows to actuate unimpeded. Similarly, a joint is also used at the distal end for the connection between the SBFA and the water-jet parts, although no flow diversion is employed in this case.

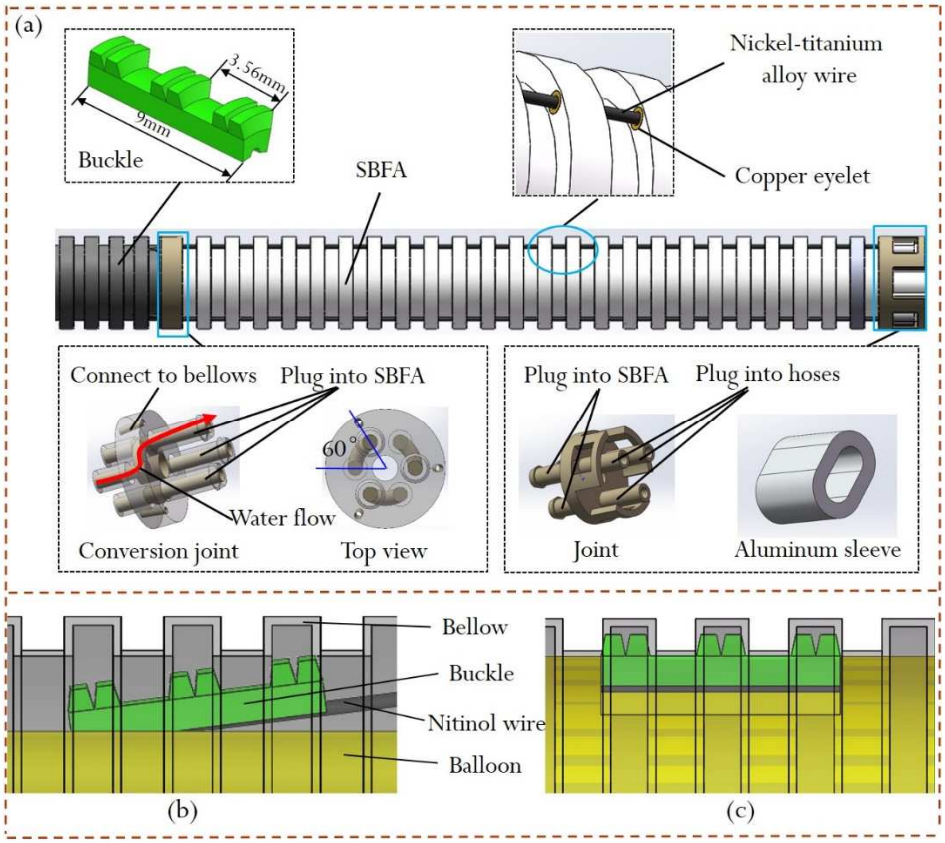

Fig. 6. (a) Structural diagram of the shape-locking mechanism. (b) Free state of the shape-locking mechanism. (c) Locking state of the mechanism.

RESULTS

Bending Characteristics of SBFA

The bending properties of SBFA were evaluated using an NDI Aurora Electromagnetic Tracking System (NDI Corp., CA). A miniature electromagnetic

sensor was attached to the tip of the endoscope, allowing to measure the angle of rotation (α).

Fig. 7 shows the relationship between the driving pressure and angle α. As shown in Fig. 7, the maximum bending angle (α) is 82°, corresponding to the 140 kPa water pressure. The observation of the cardia and the lesser curvature of the stomach requires a bending angle of 180°, which necessitate a higher water pressure; risking damage to the SBFA. Hence, the observation cannot be made purely by bending the SBFA, and thus the microvalve nozzle structure with water-jet-enhanced dual bending is utilized.

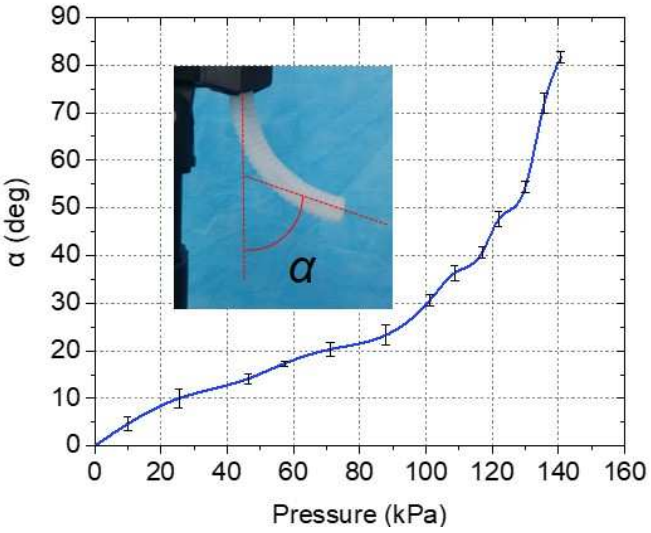

Fig. 7. Bending test results of the SBFA.

Characteristics of Microvalve

The opening pressure of the microvalve corresponds to the maximum water pressure at which the SBFA bends. To design the ideal microvalve size, a series of simulations was conducted. A single-channel valve body with a 4-mm-diameter hole (the same as in the nozzle) was designed, and then bonded to an elastic rubber membrane. During the experiment, a digital push–pull force gauge was used to measure the variation of pretension force with film displacement. The gauge was fixed on a three-axis translation stage. To simulate the pressure force in the channel, a base with a 1.6-mm cylindrical loading stick was used, which was connected and fixed to the head of a digital push–pull force meter. A passive arm (Magic Arm, XYZ, USA) was used to fix the valve body. By adjusting the three-axis translation stage, the loading stick and the valve body were placed coaxially and allowed to contact slightly. The setup is shown in Fig. 8(a), and the relationship between the force and displacement is plotted in Fig. 8(b).

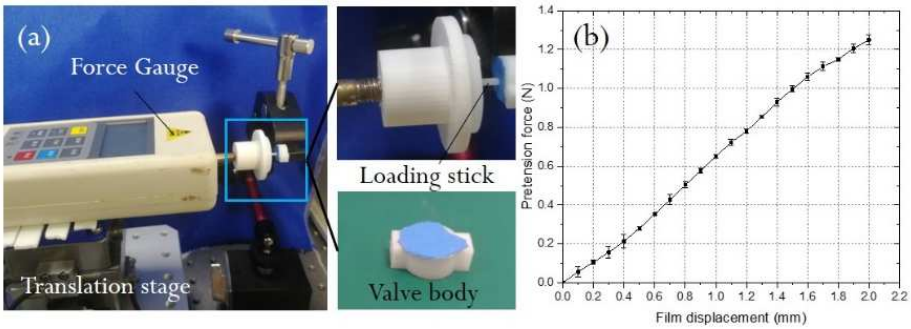

Fig. 8. (a) Membrane pretension force test setup. (b) Test results.

As shown in Fig. 8(b), the relationship between the pretension force and film displacement of the microvalve is approximately linear. When the water pressure reaches 140 kPa, a pressure force of 1.12 N works on the elastic rubber membrane. From this relationship, the displacement is approximately 1.7 mm when the pretension force is approximately 1.12 N. Therefore, the convex length of the miniature valve is 1.7 mm. Meanwhile, the opening pressure is approximately equal to the maximum pressure of the SBFA. Thus, the SBFA can be used to bend and reduce the amount of water entering the human body without structural damage.

The characteristics of the microvalve were also evaluated. First, the water pressure was gradually increased until the microvalve opened. Second, the pressure was gradually decreased until the microvalve closed. Changes in water pressure and flow rate during this process were recorded. Fig. 9 shows the test results of the relationship between the inner pressure and flow rate of the microvalve. The black and red arrows indicate the direction of pressure change. These data confirm that the fluid passes through the valve only after reaching a specific pressure value.

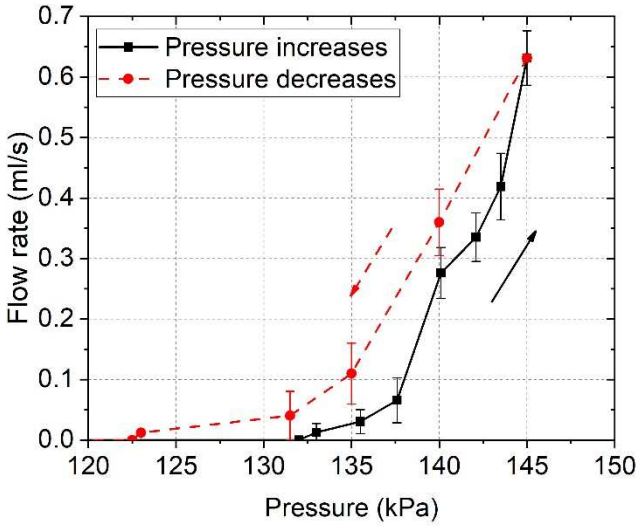

Fig. 9. Pressure vs. flow rate of water.

From Fig. 9, water starts to flow at 133 kPa. Meanwhile, the microvalve opens. As the pressure increases, the opening becomes larger and so does the flow rate of water. The microvalve gradually closes as the water pressure decreases, reducing the flow rate of water. Finally, at approximately 123 kPa, the water stops flowing and the microvalve is shut. The experiments reveal that the dimensions of the microvalve meet the design requirements and are more compatible with the SBFA.

Force Generated by Water-jet

To avoid injuring the patient's stomach during the scanning procedure, the contact pressure between the endoscopic device and the stomach should be less than 3 bar [30]. Therefore, it is necessary to measure if the water pressure meets the safety regulations. We measured the force generated by the water-jet using a digital force gauge. The measurement setup and results are shown in Fig. 10. The pressure was increased by adjusting the pressure-regulating valve until the microvalve opened and the nozzle began to spray water. Meanwhile, the digital push–pull force gauge started to record data. The water pressure was slowly increased to gauge the change in the force generated by the water-jet.

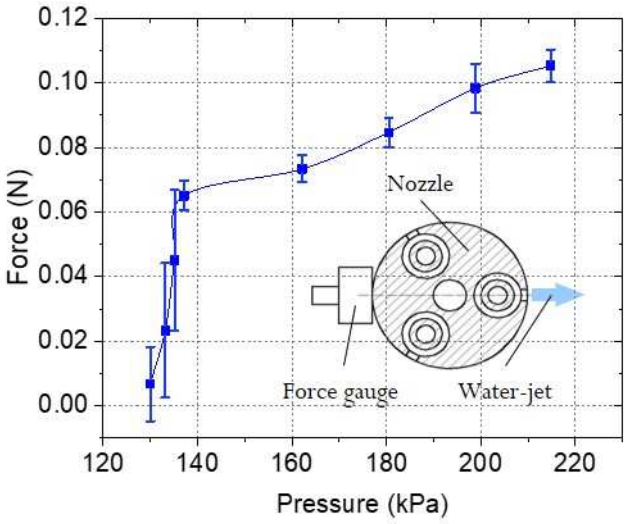

Fig. 10. Water-jet force test setup and results.

As shown in Fig. 10, when the water pressure was approximately 138 kPa, a driving force reaching 0.06 N was exerted on the nozzle, opening the microvalve. As the water pressure continues to increase, the water-jet force also gradually increases. Meanwhile, the maximum water-jet power does not exceed 0.1 N (the water pressure of the actual device should not be greater than 200 kPa, to prevent damage). The maximum pressure of the system working on the human tissue is 0.318 bar, which is far less than the upper limit of 3 bar that the human body can withstand. In summary, the water-jet system designed in this study is safe for the human body and can be used for gastrointestinal (GI)-tract screening.

Workspace Evaluation

The NDI Aurora Electromagnetic Tracking System was also used to evaluate the range of tip motion. A miniature electromagnetic sensor was placed in the middle of the nozzle to measure its tip position (Fig. 11(a)). In the flexible state, the endoscope was actuated in all possible directions by pressurized water. The ambient temperature of the experiment was 37□, which is similar to the normal temperature of the human body. The ranges of motion at different water pressures (80, 115, and 135 kPa) are shown in Fig. 11(b)–(d). From the results, the nozzle completed the ring scan with the help of three microvalves. Different pressures have different scanning ranges. By incorporating different pressures, the nozzle can cover an ellipsoidal space range.

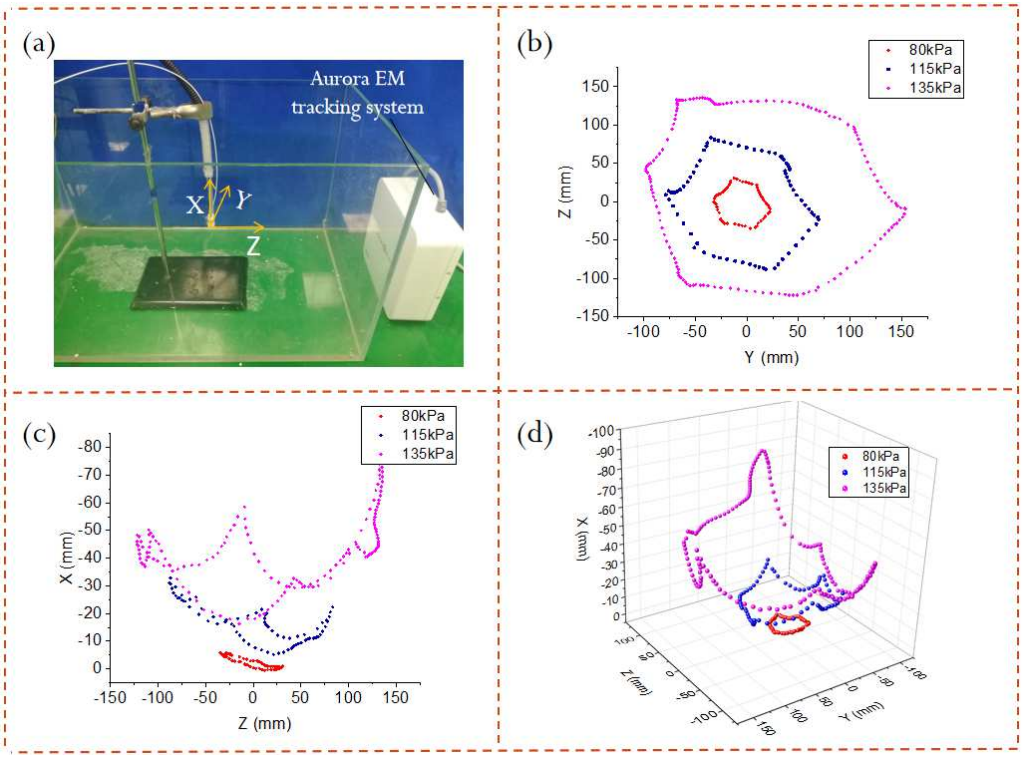

Fig. 11. (a) Experimental setup. (b) Horizontal workspace projection. (c) Lateral workspace projection. (d) The full semi-hemispherical workspace at different water pressures.

To compare the ranges of motion achieved with and without water-jet, water pressure was increased until the formation of the water-jet. The same method was used to measure the ranges of motion. The experimental results are shown in Fig. 12. A comparison of these results with those of the soft bending motion under the pressure of 135 kPa revealed an increase in the range of motion. Meanwhile, this motion also covers an ellipsoidal area of range. Fig. 12 (d) shows the results of a single-channel water-jet motion. The device traverses along an approximate elliptical surface, and the water-jet extends the range of motion. In Fig. 12(c), enhancement by the water-jet is accompanied with a horizontal workspace projection radius of approximately 150 mm, which satisfies the design criterion. Without water-jet enhancement, however, the system does not fulfil the criterion. The calculation of area under the curve revealed a 58% increase in the workspace of the endoscope upon the introduction of the water-jet.

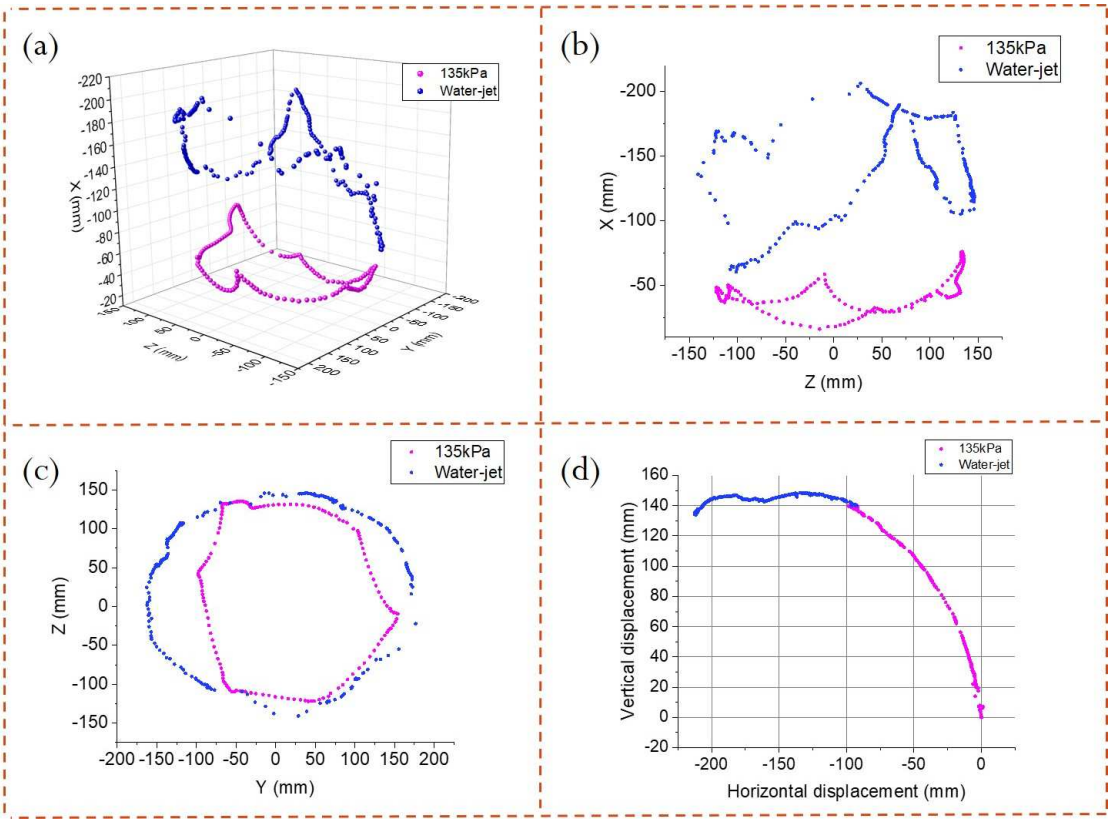

Fig. 12. (a) Full semi-hemispherical workspace comparison. (b) Lateral workspace projection. (c) Horizontal workspace projection. (d) Single-channel comparison of workspace.

Shape-locking Evaluation

The stiffness of the endoscope in both flexible and rigid states was evaluated. The device was supported by two holding points (Fig. 13(a)), and the point span was set to 50 mm. The load was applied horizontally to the middle of the shaft in the right side of the X-axis. A force gauge with an X-axis stage was used to measure the loading force and deflection displacements. Each experiment was repeated three times. As shown in Fig. 13(b), the maximum load in the rigid state was 0.54 N with a 21 mm deflection displacement. In contrast, the maximum load in the flexible state was only 0.17 N with the same 21 mm deflection displacement. The stiffness in the rigid state was approximately 3.2 times more than that in the flexible state when the deflection of the shaft was 21 mm. In other words, shape locking mechanism of the device can reach 220% stiffness variation, which is far better than the 36% variation using convectional negative pneumatic method [35].

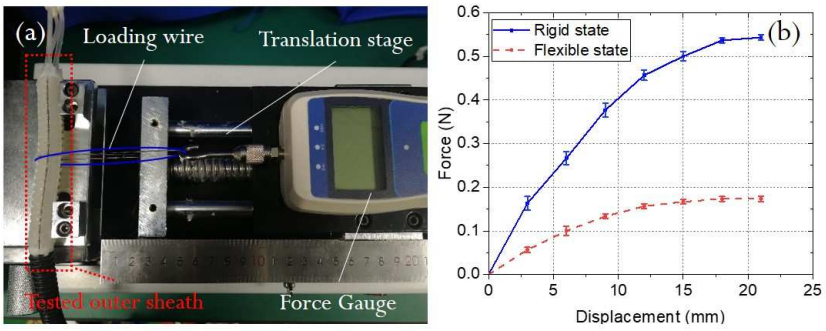

Fig. 13. (a) Endoscope stiffness test setup. (b) Force–displacement test results of the endoscope.

The shape-locking ability of the endoscope was also evaluated (Fig. 14). In the flexible state, the endoscope has high flexibility, which cannot remain linear because of the influence of its own gravity. In the rigid state, the maximum force under which the device did not undergo any obvious changes in deformation was 0.6 N (60 g) at a displacement of 95 mm. Thus, the maximum torque for shape locking was 5.7 Ncm. With same outer diameter, the shape-locking ability in this work is better than the liquid metal based method [36], which was 4 Ncm.

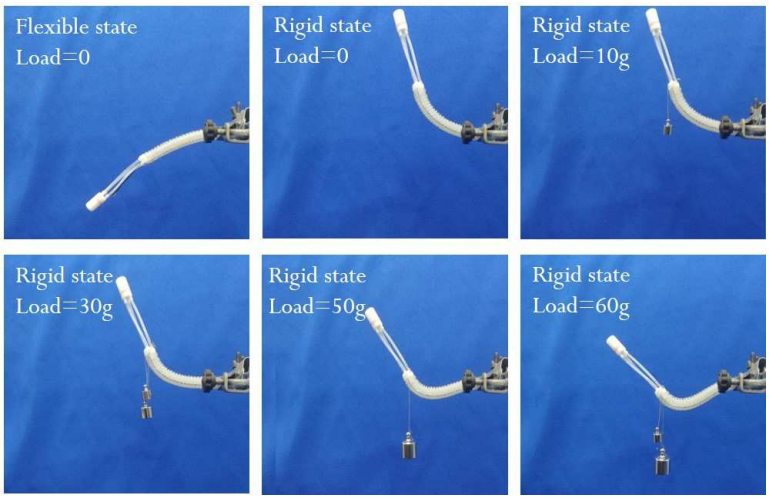

Fig. 14. Shape-locking function test.

Phantom Experiment

This experiment was performed to compare the performance of the new system with that of a conventional flexible endoscope (GIF TYPE 2TQ260, OLYMPUS, Japan). The operator performed five phantom experiments. The phantom region was a hemispherical space with five landmarks for target observation (white color foam with an area of approximately 25 mm^2). Four participants were invited to complete the

experiments using a traditional endoscope and the new dual-bending endoscope separately. For the dual-bending endoscope, an internal camera (Shenzhen ezon Corp., 4mm diameter, 14.5mm length, 75° field of view angle, 1M pixels) with a light source was fixed on the distal nozzle for capturing images. Participants were trained until they could skillfully operate the device. We subsequently compared the time taken to complete the experiment using the new device with that using a traditional endoscope.

The user was directed to determine all five points of interest and perform the experiment five times. The points can be observed by the internal camera of the prototype and the endoscope, as shown in Fig. 15. To negate the influence of memory bias on the results, the points for each trial were chosen arbitrarily. The average time to complete the trial required for this process is listed in Tab. III.

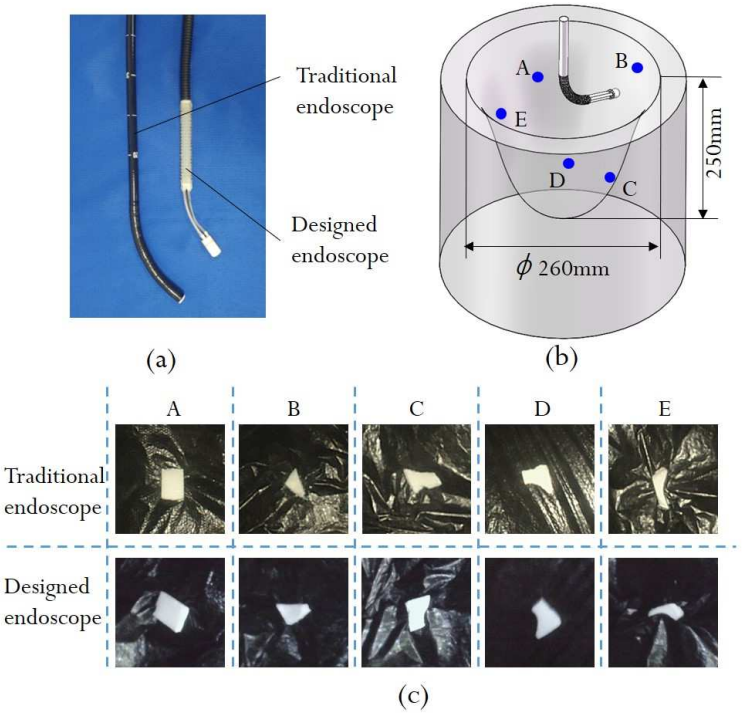

Fig. 15. (a) Comparison of traditional and the designed endoscope. (b) Setup of the phantom experiment. (c) Images from traditional and the designed endoscope.

Table III. Comparison of results of the trials between the new device and the standard endoscope.

		Time(seconds)	Standard Deviation(seconds)
Before training	Endoscope	103	19
	Water-jet-enabled device	286	19
After training	Water-jet-enabled device	198	16

The experimental results showed that the time taken by novice technicians to complete an experiment with the new device was approximately 2.8 times longer than with the endoscope. However, the completion time can be minimized (by 31%) after training the technicians sufficiently. Although the prototype still requires a longer time than the flexible endoscope to complete a trial, these results fell within the typical time range of a gastroscopic procedure (approximately 900 s for one procedure), and can be further improved by introducing better control interfaces and providing technicians with further training to operate the medical device.

DISCUSSION

In this study, we developed a novel dual-bending hydraulic endoscope to assist with gastric cancer screening. The device is actuated by pressurized water. The novelty of the endoscope is that it bends the gastric screening device to achieve greater viewing angles. The device possesses the function of shape-locking, which is basically the ability of the device's distal tip to move while its body is locked in place. This function can be achieved by a mechanism consisting of pneumatic balloons, wires, bellows, and buckles. The endoscope employs a specially designed microvalve, to switch between the single bending of SBFA and water-jet-enhanced dual bending of the device tip. The introduction of water-jet increased the workspace of the endoscope by 58%.

In this study, the SBFA was manufactured by casting the Dragon Skin 20 silicone rubber in a 3D-printed mold. Dragon Skin 20 has good ductility and strength. The accuracy of the mold as well as human errors during molding made it difficult to fabricate the SBFA with higher precision. We designed three chambers in the SBFA with varying wall thickness and shape, which gave it an asymmetric bending range. A more precise processing technology or method must be adopted in future research. A pressure-regulating valve was employed to regulate the air pressure in the water tank.

For the workspace experiment, maximum bending angle (α) of the SBFA was 82°, and the corresponding water pressure was approximately 140 kPa. With help of water-jet, horizontal workspace projection radius after the incorporation of a water-jet was approximately 150 mm. The stomach of the average adult has a maximum width of 10 cm and a length of 34 cm at the greater curvature [33]. The workspace combined with the field of view of the camera (75°) and the difference insertion length should be sufficient for observing most parts of the greater curvature of the stomach. The opening

of the microvalve can make the device bend by an adequately large angle, enabling the physician or technician to directly observe the cardia and the lesser curvature of the stomach.

As the SBFA acts in conjunction with the water-jet driven tip, even with varied insertion lengths, the endoscope can reach a wide range of bending angles. Ultimately, the insertion degree of freedom may be operated by the trained user to perform the screening procedure most effectively. Considering the more than 1000cm^3 space and 34cm greater curvature length of an average adult's stomach, we think the 20cm bending length is acceptable. In addition, benefiting from shape-locking ability of the proposed device, the SBFA can be firstly actuated and then locked. The water-jet actuation is started for local scanning afterwards. When the SBFA is locked, the bending length is shortened to about 10cm, which is similar with commercial endoscopes. Based on the presented testing, 200 mm length was found to be suitable, however, for alternative scenarios, the SBFA and water-jet section lengths (and therefore overall lengths) may be adjusted without significant design alteration.

Although system stability was suitable for the benchtop visualization tasks performed, it has also been demonstrated using kinematic model design [14] and improved flow control hardware [15] that stability and controllability for water-jet systems may be further improved. As part of our future work, we will explore these and other methods to further improve the efficacy of the device.

For the shape-locking experiments, the maximum shape-locking torque in the rigid state was 5.7 Ncm. The maximum force of the water-jet did not exceed 0.1 N, which is within the load-bearing range of the rigid state. This implies that this torque meets the stability criterion of the SBFA with water-jet. The balloon was used to lock the wire in place and fix the shape. The structure is simple and operates rapidly (approximately 2 s). The device is soft, and therefore can be easily detached from the human body in case of an emergency.

We performed a phantom experiment and engaged and trained a group of people to fill the role of device technicians. It took a longer time for the technicians to the complete a trial with the proposed endoscope (an average of 286 s) than with the conventional endoscope. With proper training, the technicians can shorten this time to 198 s. With the average time of 900 s taken to complete the gastroscopy procedure, the

efficiency of the new device can be considered acceptable. In addition, the camera had a narrower field of view (75° vs. 140°) and a shorter focus distance (3–80 mm vs. 3–100 mm) than the conventional endoscope, which partly contributes to the time difference between the completion of the procedure by the two devices. The workspace and shape-locking evaluations show that the endoscope can be actuated in the stomach for large-area scanning and provide a stable platform for local scanning. The maximum force generated by the water-jet was 0.1 N, which is safe for the stomach because the force level for manipulating stomach tissues should be higher than 2N [37]. The maximum water-jet pressure of 0.318 bar at the nozzle ports is also safe compared with the threshold of 3 bar [34].

The demonstrated workspace scanning of the proposed endoscope represents suitable coverage for stomach screening. In addition, the reversible shape-locking functionality and portable and low cost deign make the endoscope well suited for gastric cancer scanning in low- and middle-income regions. Specifically, the hardware cost of the proposed endoscope together with the camera falls under 800 USD total (<$40 for single use parts), which is much lower than traditional endoscopes. The endoscope along with the water tank system and the controlling parts can be packaged into the size of a standard luggage container (0.2 m^3, 10 kg), making it compact and easily transportable.

Future work will focus on improving the stability of the water-jet, preferably by using optimized control algorithms to regulate the pressure/flow of water. In addition, design refinement to further minimize size and cost of the endoscope and control system will be explored. The employment of multi-lumen tubing and integration of an air pump, water tank, and controlling valves will be explored to this end. Finally, a separate channel with a nozzle jetting water directly on to the lens will be integrated to allow selective camera lens cleaning, which can become blurred with blood or mucus in the scanning process.

CONCLUSIONS

In this paper, we detail the development of a new dual-bending hydraulic endoscope with shape-locking mechanism for gastric screening. A microvalve was designed to switch between the single bending of the SBFA and water-jet-enhanced dual bending of the device tip. With 135 kPa water pressure, horizontal workspace projection radius

after the incorporation of a water-jet was approximately 150 mm, suitable for coverage of an average adult stomach. A 58% increase in the workspace after introduction of the water-jet was achieved. In the rigid state, the SBFA locked the shape of the device to improve the stability of the water-jet's bending motion. The stiffness in the rigid state (5.7Ncm) was approximately 3.2 times more than that in the flexible state. The experimental results demonstrated the potential clinical value of the endoscope in improving the prospects for upper gastrointestinal tract disease screening, especially gastric cancer.

FUNDING

This work was supported in part by National Key R&D Program of China under Grant No. 2019YFB1311501, in part by National Natural Science Foundation of China under Grant No. 51905374 & 61773280 and in part by Engineering and Physical Sciences Research Council under Grant No. EP/P027938/1.

CONFLICT OF INTEREST

The authors declare that they have no conflict of interest.

INFORMED CONSENT

This article does not contain patient data.

ETHICAL APPROVAL

Not applicable.

REFERENCES

[1] Bray F, Ferlay J, Soerjomataram I, et al. (2018). Global Cancer Statistics 2018: GLOBOCAN Estimates of Incidence and Mortality Worldwide for 36 Cancers in 185 Countries. CA: A Cancer Journal for Clinicians 2018;0:1-31.

[2] Ferlay J, Soerjomataram I, Dikshit R, et al. Cancer incidence and mortality worldwide: sources, methods and major patterns in GLOBOCAN 2012. International Journal of Cancer, 2015, 136(5):E359-E386.

[3] Ferlay J, Shin H R, Bray F, et al. Estimates of worldwide burden of cancer in 2008: GLOBOCAN 2008. International Journal of Cancer, 2010, 127(12):2893-917.

[4] Lee K J, Inoue M, Otani T, et al. Gastric cancer screening and subsequent risk of gastric cancer: a large-scale population-based cohort study, with a 13-year follow-up in Japan. International Journal of Cancer, 2006, 118(9):2315–2321.

[5] Adami H-O, Day N E, Trichopoulos D, et al. Primary andsecondary prevention in thereduction of cancer morbidity and mortality. Eur. J. Cancer, 2001, 37: S118–S127.

[6] Office of Inspector General. Healthcare inspection. Use and reprocessing of flexible fiberoptic endoscopes at VA medical facilities. Washington (DC): U.S. Department of Veterans Affairs; 2009, 09–01784-146:1–45.

[7] Petersen B T, Chennat J, Cohen J, et al. Multisociety Guideline on Reprocessing Flexible GI Endoscopes: 2011. Gastrointest Endosc 2011,73:1075-84.

[8] Bray F, Jemal A, Grey N, et al. Global cancer transitions according to the human development index: A population-based study. Lancet Oncol 2012, 13:790–801.

[9] Kang D, Lim CH, Choi MG, Lee H, Kim JS, Cho YK, et al. An Operable, Portable, and Disposable Ultrathin Endoscope for Evaluation of the Upper Gastrointestinal Tract. Digestive Diseases and ences 2019.

[10] Dominitz JA, Johnston RS, Melville CD, Kimmey MB, Seibel EJ. Low-Cost Tethered Capsule Endoscope (TCE) for Unsedated Esophagoscopy. Gastrointest Endosc 2007; 65.

[11] Ye X, Cabibihan JJ, Yoon WJ. Design and verification of a flexible device for steering a tethered capsule endoscope in the stomach. 2017 14th International Conference on Ubiquitous Robots and Ambient Intelligence (URAI) 2017.

[12] Chandler JH, Chauhan M, Caló S, Aruparayil N, Valdastri P. Tu1964 Usability of a Novel Disposable Endoscope for Gastric Cancer Screening in Low-resource Settings: Results from Rural India. Gastroenterology 2020; 158:1235.

[13] Nicolo, Garbin, Long, Wang, James, H, et al. Dual-Continuum Design Approach for Intuitive and Low-Cost Upper Gastrointestinal Endoscopy. IEEE Transactions on Bio Medical Engineering 2018.

[14] Caprara R, Obstein KL, Scozzarro G, et al. A platform for gastric cancer screening in low- and middle-income countries. IEEE Trans. Biomed. Eng. 2015; 62(5): 1324–1332.

[15] Calo S, Chandler JH, Campisano F, Obstein KL, Valdastri P. A Compression Valve for Sanitary Control of Fluid-Driven Actuators. IEEE/ASME Transactions on Mechatronics 2020; 25:1005-15.

[16] Campisano F, Remirez AA, Calo S, Chandler JH, Obstein KL, Webster RJ, et al. Online Disturbance Estimation for Improving Kinematic Accuracy in Continuum Manipulators. IEEE ROBOTICS AND AUTOMATION LETTERS 2020; 5:2642-9.

[17] Campisano F, Gramuglia F, Dawson IR, et al. Gastric Cancer Screening in Low-Income Countries: System Design, Fabrication, and Analysis for an Ultralow-Cost Endoscopy Procedure. IEEE Robot Autom Mag.2017(Jun); 24(4):73-81.

[18] Yin L, Wang S, Zuo S. Water-jet outer sheath with braided shape memory polymer tubes for upper gastrointestinal tract screening. Int J Med Robot Comp 2018; 14.

[19] Burgner-Kahrs J, Rucker DC, Choset H. Continuum Robots for Medical Applications: A Survey. Ieee T Robot 2015; 31:1261-80.

[20] Veiga TD, Chandler JH, Lloyd P, Pittiglio G, Valdastri P. Challenges of continuum robots in clinical context: a review. Progress in Biomedical Engineering 2020.

[21] Rus, Daniela, Tolley, M. T. Design. fabrication and control of soft robots. Nature 2015 521.7553: 467-475.

[22] Noritsugu T, Takaiwa M, Sasaki D. Power Assist Wear Driven with Pneumatic Rubber Artificial Muscles. International Conference on Mechatronics and Machine Vision in Practice. IEEE, 2008:539-544.

[23] Bertetto A M, Ruggiu M. A novel fluidic bellows manipulator. J Robot Mechatron.2004; 16 (6): 604-612.

[24] Lindenroth L, Althoefer K, Rhode K, et al. Design and Control of a Soft Robotic Endoscope for Surgical Interventions utilizing Hydraulic Actuation. The, Hamlyn Symposium on Medical Robotics. 2016.

[25] Ikuta K, Ichikawa H, Suzuki K, et al. Safety active catheter with multi-segments driven by innovative hydro-pressure micro actuatorS. IEEE the Sixteenth International Conference on MICRO Electro Mechanical Systems, 2003. Mems-03 Kyoto. IEEE, 2003:130-135.

[26] Amir D, Howie C, Alon W, Takeyoshi O, Marco AZ. Percutaneous intrapericardial interventions using a highly articulated robotic probe. In: The first IEEE/RAS-EMBS international conference on biomedical robotics and biomechatronics; 2006. p. 7–12.

[27] Zuo S, Masamune K, Kuwana K et al. Nonmetallic rigidflexible outer sheath with pneumatic shapelocking mechanism and double curvature structure. Med Image

Comput Comput Assist Interv –MICCAI 2011, Lecture Notes in Computer Science 2011; 6891:169–177.

[28] Zuo S, K Iijima, T Tokumiya, K Masamune. Variable stiffness outer sheath with ‘‘Dragon skin’’ structure and negative pneumatic shape-locking. Int. J. Comput. Assist. Radiol. Surg. 2014; 9(5):857–865.

[29] Kim YJ, Cheng S, Kim S, Iagnemma K. A stiffness adjustable hyperredundant manipulator using a variable neutralline mechanism for minimally invasive surgery. IEEE Trans Robot 2014; 29(4):1031–1042.

[30] Ranzani T, Cianchetti M, Gerboni G, De Falco I, Menciassi A. A Soft Modular Manipulator for Minimally Invasive Surgery: Design and Characterization of a Single Module. IEEE T Robot 2016; 32:187-200.

[31] Brancadoro M, Manti M, Grani F, Tognarelli S, Menciassi A, Cianchetti M. Toward a Variable Stiffness Surgical Manipulator Based on Fiber Jamming Transition. Frontiers in Robotics and AI 2019; 6.

[32] Shaker R, Belafsky P C, Postma G N, et al. Principles of Deglutition. Springer New York; 2012.

[33] Hall JE, Guyton and Hall. Textbook of Medical Physiology. Elsevier New York; 2010.

[34] Moshkowitz M, Hirsch Y, Carmel I, et al. A novel device for rapid cleaning of poorly prepared colons. Endoscopy. 2010; 42(10):834-6.

[35] Cianchetti M, Ranzani T, Gerboni G, Falco ID, Menciassi A. STIFF-FLOP surgical manipulator: Mechanical design and experimental characterization of the single module. IEEE/RSJ International Conference on Intelligent Robots & Systems 2013.

[36] Peters J, Nolan E, et al. Actuation and stiffening in fluid-driven soft robots using low-melting-point 405 material. 2019 IEEE/RSJ International Conference on Intelligent Robots and Systems (IROS 2019); 406 Macau: IEEE, 2019.

[37] Ikuta K, Yamamoto K, Sasaki K. Development of remote microsurgery robot and new surgical procedure for deep and narrow space. in Proc. IEEE Int. Conf. Robot. Autom. (ICRA), Taipei, Taiwan; 2003; p. 1103–1108.